

Thomson scattering in dense plasmas with density and temperature gradients

C. Fortmann^a, R. Thiele^a, R. R. Fäustlin^b, Th. Bornath^a, B. Holst^a, W.-D. Kraeft^a, V. Schwarz^a, S. Toleikis^b, Th. Tschentscher^b, R. Redmer^a

^a*Institut für Physik, Universität Rostock, 18051 Rostock, Germany*

^b*Deutsches Elektronensynchrotron DESY, Notkestrasse 85, 22607 Hamburg, Germany*

Abstract

Collective X-ray Thomson scattering has become a versatile tool for the diagnostics of dense plasmas. Assuming homogeneous density and temperature throughout the target sample, these parameters can be determined directly from the plasmon dispersion and the ratio of plasmon amplitudes via detailed balance. In inhomogeneous media, the scattering signal is an average of the density and temperature dependent scattering cross-section weighted with the density and temperature profiles. We analyse Thomson scattering spectra in the XUV range from near solid density hydrogen targets generated by free electron laser radiation. The influence of plasma inhomogeneities on the scattering spectrum is investigated by comparing density and temperature averaged scattering signals to calculations assuming homogeneous targets. We found discrepancies larger than 10% between the mean electron density and the effective density as well as between the mean temperature and the effective temperature.

Key words: Plasma diagnostics, radiation hydrodynamics, free electron laser

1. Introduction

Recently, X-ray Thomson scattering has been demonstrated to be a reliable and versatile tool for the diagnostics of dense plasmas [1]. Examples for applications cover a large range from laser produced plasmas at temperatures of several keV and densities between solid density and a few percent of solid density (hot dense plasmas) [2, 3] via so-called warm dense matter (WDM) [4, 5] with temperatures of several eV and densities close to solid density [6, 7], up to compressed matter at temperatures between 0.1 eV and several 10 eV [8, 9].

The determination of the plasma properties, such as the plasma density, the plasma temperature, and the plasma composition, requires the knowledge of the density and temperature dependent scattering cross-section. As will be outlined in Sec. 2, the cross-section for Thomson scattering is usually expressed via the dynamical structure factor (DSF) $S_{ee}(\mathbf{k}, \omega)$ [10],

which is a function of the scattering wavevector \mathbf{k} and the frequency shift ω , convoluted with the density and temperature distribution of the target. In this way, plasma inhomogeneities can be taken into account in the simulation of the scattering spectrum, which is the main purpose of this paper. Such analysis has been performed earlier by Baldis et al. [11] for the case of VUV photons interacting with solid aluminum targets. Here, the scenario of XUV photons delivered by the free electron laser facility at DESY-Hamburg (FLASH) [12] scattering on liquid hydrogen at near solid density (mass density $\rho = 0.088 \text{ g/cm}^3$) as proposed by Höll et al. [13], will be considered.

2. Theory of Thomson Scattering and the dynamic structure factor

The scattered power per solid angle $d\Omega = \sin \vartheta d\vartheta d\varphi$ and unit frequency interval $d\omega$ is

Email address:
carsten.fortmann@uni-rostock.de (C. Fortmann)

given by the expression [11]

$$\frac{d^2 P_{\text{sc}}}{d\Omega d\omega} = \frac{\sigma_{\text{T}}}{A_{\text{rad}}} \frac{k_{\text{f}}}{k_{\text{i}}} \int_{-\infty}^{\infty} \frac{d\omega'}{2\pi} G_{\Delta\omega}(\omega - \omega') \times \int_{V_{\text{rad}}} d^3\mathbf{r} I(\mathbf{r}) S_{\text{ee}}(\mathbf{k}, \omega'; n_{\text{e}}(\mathbf{r}), T(\mathbf{r})) n_{\text{e}}(\mathbf{r}). \quad (1)$$

$\sigma_{\text{T}} = 6.65 \times 10^{-24} \text{ cm}^2$ is the Thomson cross-section, \mathbf{k}_{i} and \mathbf{k}_{f} are the initial and the final photon wavevector, respectively. By $\mathbf{k} = \mathbf{k}_{\text{i}} - \mathbf{k}_{\text{f}}$, we denote the scattering wavevector. From the conservation of momentum, we obtain $k = 4\pi \sin(\vartheta/2)/\lambda_0$, with λ_0 being the probe wavelength. $I(\mathbf{r})$ is the \mathbf{r} dependent power density of incoming photons, while A_{rad} is the radiated surface of the target. Via the convolution of the DSF with an appropriately chosen instrumental function $G_{\Delta\omega}(\omega)$, the finite resolution of the spectrometer as well as the probe's bandwidth is taken into account. Here, we use the normalized Gaussian distribution

$$G_{\Delta\omega}(\omega) = \frac{1}{\sqrt{2\pi}\sigma} \exp\left(-\frac{\omega^2}{2\sigma^2}\right), \quad (2)$$

$\Delta\omega = 2\sqrt{2 \ln 2} \sigma$ is the full width at half maximum (FWHM) of the instrumental function.

Finally, the plasma inhomogeneities are taken into account by averaging the DSF with the electron density profile $n_{\text{e}}(\mathbf{r})$ and the temperature profile $T(\mathbf{r})$.

It is convenient to separate the DSF into contributions from free-free, free-bound and bound-bound correlations as proposed by Chihara [10],

$$S_{\text{ee}}(\mathbf{k}, \omega) = |f_{\text{i}}(k) + q(k)|^2 S_{\text{ii}}(\mathbf{k}, \omega) + Z_{\text{c}} \int_{-\infty}^{\infty} d\omega' S_{\text{c}}(\mathbf{k}, \omega) S_{\text{s}}(\mathbf{k}, \omega - \omega') + Z_{\text{f}} S_{\text{ee}}^0(\mathbf{k}, \omega). \quad (3)$$

The first part gives the correlation of electrons that are weakly and tightly bound to the ions and follow the ion's movement adiabatically. The amplitude is determined by the atomic form factor $f_{\text{i}}(k)$, i.e. the charge distribution of the electrons in the valence shell orbitals and the screening cloud $q(k)$ which gives the distribution of quasi-free electrons screening the ion's charge [14].

The second term contains the contribution of core electrons, $S_{\text{c}}(\mathbf{k}, \omega)$ and describes Raman type transitions of inner shell electrons to the continuum, modulated by the ion's movement which is contained in $S_{\text{s}}(\mathbf{k}, \omega)$ [15].

Finally, $S_{\text{ee}}^0(\mathbf{k}, \omega)$ is the free electron contribution. It determines the behaviour of the total electron structure factor at frequencies close to the plasma frequency. Since we focus on the application of Thomson scattering to diagnostics of dense plasmas via analysis of the plasmon feature, the third term in Eq. (3) will be discussed in more detail in the following. This contribution is calculated in the Born-Mermin approximation [16], thereby including collisions among electrons and ions in second order Born approximation. Higher order terms can be treated via the t-matrix and inclusion of dynamical screening, see Ref. [17]. The influence of collisions on the collective scattering spectrum has been thoroughly discussed by some of the authors in Ref. [18]. In this paper, we will concentrate on the impact of the density and temperature profiles on the scattering signal.

3. Temperature and density profiles

We consider the interaction of cryogenic ($T \simeq 20 \text{ K}$) liquid hydrogen droplets of about $30 \mu\text{m}$ diameter with XUV free electron laser radiation delivered by FLASH at 13.5 nm wavelength with a pulse length of 30 fs and $50 \mu\text{J}$ pulse energy. In order to infer the absorption characteristics of the target, we calculate the inverse absorption length $\alpha(\omega)$ of cryogenic hydrogen ($T = 20 \text{ K}$) via ab-initio quantum molecular dynamic simulations using the Kubo-Greenwood formula [19]. The inverse absorption length as a function of the photon energy is shown in Fig. 1. At the FLASH energy (92 eV , indicated by the red arrow) the absorption length is $15 \mu\text{m}$, in excellent agreement with tabulated x-ray absorption data [20], which is in the same order of magnitude as the diameter of the hydrogen droplet. Thus, FLASH photons can penetrate deeply into the target.

The interaction of FLASH photons with the hydrogen target was simulated using the radiation-hydrodynamic simulation code HELIOS [21]. HELIOS features a Lagrangian reference frame, separate ion and electron temperatures, and flux-limited Spitzer thermal con-

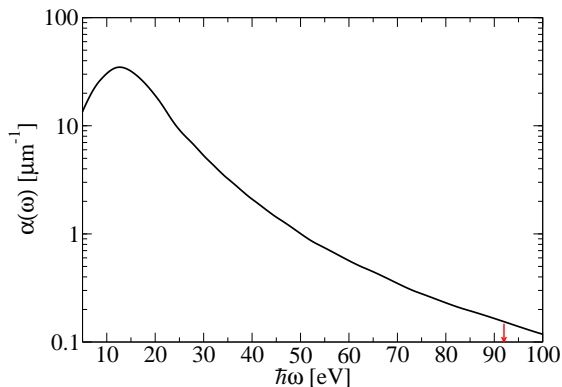


Figure 1: (Color online) Ab-initio simulation of the inverse absorption length for cryogenic hydrogen at solid density as a function of the photon energy. The red arrow indicates the FLASH energy (92 eV).

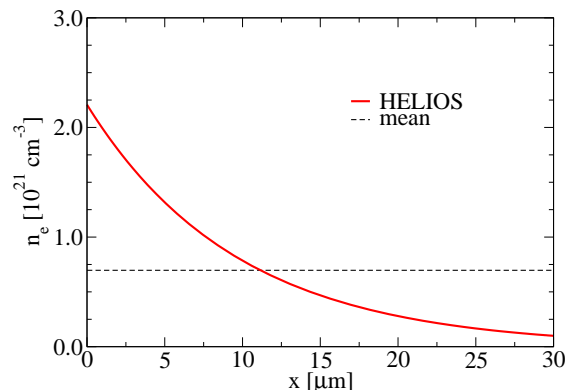
ductivity. It allows for deposition of laser energy via inverse bremsstrahlung as well as bound-bound and bound-free transitions, using a SESAME-like equation of state.

Figure 2 shows the free electron density profile (a) and temperature profile (b) (red solid curves). The density profile decreases exponentially from $n_e = 2.2 \times 10^{22} \text{ cm}^{-3}$ at the irradiated surface ($x = 0$) to $n_e = 1.0 \times 10^{20} \text{ cm}^{-3}$ at the rear surface ($x = 3.0 \mu\text{m}$). The $1/e$ -decay length of the exponential profile is roughly $11 \mu\text{m}$, which is consistent with the absorption length obtained from the QMD simulation, c.f. Fig. 1, i.e. the absorption is mainly due to bound-free transitions.

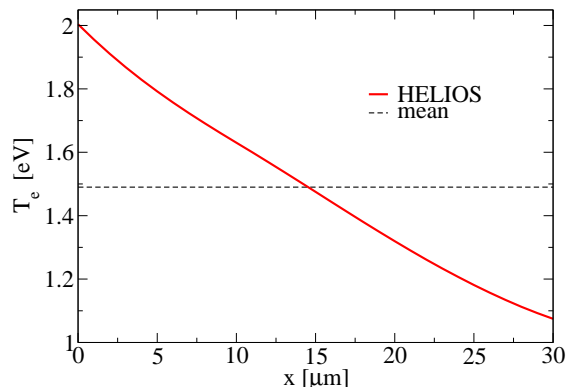
The plasma temperature decreases from $T = 2 \text{ eV}$ to $T = 1.1 \text{ eV}$. For comparison, the dashed lines indicate the mean electron density $\bar{n}_e = 7.0 \times 10^{21} \text{ cm}^{-3}$ and mean temperature $\bar{T} = 1.5 \text{ eV}$, respectively.

4. Results

In Fig. 3, we show calculations of the scattered intensity as a function of the photon energy shift with respect to the FLASH photon energy, assuming FLASH photons scattering from partially ionized hydrogen under an angle of $\vartheta = 90^\circ$. The thin curves show calculations of the scattering spectrum using a single density and temperature combination corresponding to a particular position x in the HELIOS profiles, see Fig. 2. Scattering from plasma regions close to the front surface (high density, high temperature) results in a comparatively



(a) Density



(b) Temperature

Figure 2: (Color online) Density (a) and temperature (b) profile from HELIOS simulation of liquid hydrogen droplet irradiated by XUV-FEL pulses, $\lambda_0 = 13.5 \text{ nm}$, pulse length 30 fs, pulse energy $50 \mu\text{J}$ (bold red curves). The dashed curves indicate the corresponding mean density and temperature.

large plasmon resonance energy, while scattering from the rear surface (low density, low temperature) gives rise to small plasmon energies, as indicated by the arrows and the corresponding electron densities. Finally, the bold red curve gives the density and temperature averaged scattered intensity, c.f. Eq. (1). Note, that since the DSF is weighted with the local density $n_e(\mathbf{r})$, i.e. with the number of scattering electrons in the unit volume $d^3\mathbf{r}$, as well as with the number of photons in that volume, regions close to the irradiated surface with increased density contribute more strongly to the spectrum than the dilute parts located towards the rear surface. This results in a scattering spectrum that is significantly more broadened than the original spectra taken at constant density and temperature.

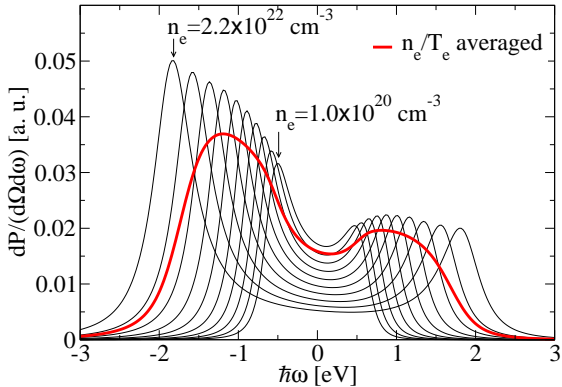


Figure 3: (Color online) Thin curves: Scattered intensity spectra at constant density and temperature corresponding to the HELIOS profiles (Fig. 2). Bold red curve: Density and temperature averaged scattering spectrum. Scattering angle $\vartheta = 90^\circ$.

We compare the averaged spectrum to a calculation for the DSF using homogeneous density and temperature distributions. The result is shown in Fig. 4. The bold red curve is again the DSF averaged with the HELIOS profiles as in Fig. 3, the black dashed curve gives the DSF using the effective electron density $n_{\text{eff}} = 8.3 \times 10^{20} \text{ cm}^{-3}$ and effective temperature $T_{\text{eff}} = 1.7 \text{ eV}$, which are inferred via the peak position of the plasmon resonances and the detailed balance analysis of the profile-averaged spectra (red curve). Both, effective density and effective temperature deviate significantly (i.e. more than 10%) from the corresponding mean values $\bar{n}_e = 7.0 \times 10^{20} \text{ cm}^{-3}$ and $\bar{T} = 1.5 \text{ eV}$. Also note that in different setups, e.g. excitation of the plasma via intense optical laser radiation, stronger density and temperature gradients are observed [22], and even larger deviations between the effective values and the mean values for n and T may occur. A further interesting observation is that the peaks of the averaged spectrum (Fig. 4) are not symmetrically located with respect to the incident photon energy as would be the case for a homogeneous temperature and density distribution in the target.

5. Conclusions

We simulated Thomson scattering spectra including density and temperature gradients in the target. By comparing these spectra to calculations that assume homogeneous den-

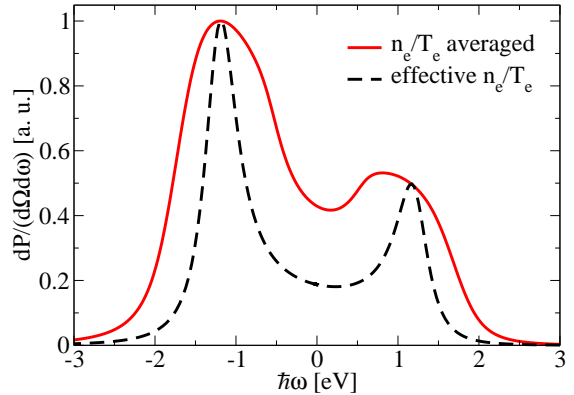


Figure 4: (Color) Density and temperature averaged scattering spectrum (bold red curve) compared to a calculation using the effective density and temperature (dashed curve) obtained from the plasmon peak positions and detailed balance analysis from the profile-averaged spectrum. Scattering angle $\vartheta = 90^\circ$.

sity and temperature distributions, we found significant differences between these methods. In particular, the free electron density that is inferred from the simulated spectrum via the plasmon dispersion, as well as the effective temperature, inferred via detailed balance analysis of the simulated spectrum may not be interpreted as the mean values of these observables. In the scenario studied here (FLASH photons at 13.5 nm wavelength scattering on near solid density hydrogen heated by the same photons), both n_{eff} and T_{eff} differ by more than 10% from the corresponding mean value.

Besides being important for the determination of density and temperature as demonstrated in this paper, deconvolution of the scattering spectra and the profiles is also crucial if one is interested in the broadening of the plasmon satellites due to collisions and Landau damping [18]. Collisional broadening of plasmons gives valuable information about the electrical and thermal conductivities in the plasma and is thus an important feature of the scattering spectrum. However, neglecting the homogeneous broadening due to the density and temperature gradients may lead to significant underestimation of the conductivity. Thus, gaining information about the density and temperature profile of the target, e.g. via radiation hydrodynamic simulations, is indispensable for the application of Thomson scattering spectra to plasma diagnostics.

Acknowledgments

This work was partly supported by the Deutsche Forschungsgemeinschaft (DFG) under Grant SFB 652 “Strong correlations and collective phenomena in radiation fields: Coulomb systems, Cluster, and Particles”, by the DFG-Graduiertenkolleg 1355 (RRF), and the German Federal Ministry of Education and Research (BMBF) under Grant FSP 301-FLASH, project No. 05 KS7HRA.

References

- [1] S. H. Glenzer, R. Redmer, *Rev. Mod. Phys.* (accepted).
- [2] S. H. Glenzer, W. Rozmus, B. J. MacGowan, K. G. Estabrook, J. D. De Groot, G. B. Zimmerman, H. A. Baldis, J. A. Harte, R. W. Lee, E. A. Williams, B. G. Wilson, Thomson scattering from high- z laser-produced plasmas, *Phys. Rev. Lett.* 82 (1) (1999) 97.
- [3] G. Gregori, S. Glenzer, H.-K. Chung, D. Froula, R. Lee, N. Meezan, J. Moody, C. Niemann, O. Landen, B. Holst, R. Redmer, S. Regan, H. Sawada, Measurement of carbon ionization balance in high-temperature plasma mixtures by temporally resolved x-ray scattering, *J. Quant. Spectrosc. Radiat. Transfer* 99 (2006) 225–237.
- [4] R. W. Lee, H. A. Baldis, R. C. Cauble, O. L. Landen, J. S. Wark, A. Ng, S. J. Rose, C. Lewis, D. Riley, J.-C. Gauthier, P. Audebert, Plasma-based studies with intense x-ray and particle beam sources, *Laser Part. Beams* 20 (3) (2003) 527–536.
- [5] R. W. Lee, S. J. Moon, H.-K. Chung, W. Rozmus, H. A. Baldis, G. Gregori, R. C. Cauble, O. L. Landen, J. S. Wark, A. Ng, S. J. Rose, C. L. Lewis, D. Riley, J.-C. Gauthier, P. Audebert, Finite temperature dense matter studies on next-generation light sources, *J. Opt. Soc. Am. B* 20 (4) (2003) 770–778.
- [6] S. H. Glenzer, G. Gregori, R. W. Lee, F. J. Rogers, S. W. Pollaine, O. L. Landen, Demonstration of spectrally resolved x-ray scattering in dense plasmas, *Phys. Rev. Lett.* 90 (17) (2003) 175002.
- [7] S. H. Glenzer, O. L. Landen, P. Neumayer, R. W. Lee, K. Widmann, S. W. Pollaine, R. J. Wallace, G. Gregori, A. Höll, T. Bornath, R. Thiele, V. Schwarz, W.-D. Kraeft, R. Redmer, Observations of plasmons in warm dense matter, *Phys. Rev. Lett.* 98 (6) (2007) 065002.
- [8] S. H. Glenzer, P. Neumayer, T. Döppner, O. L. Landen, R. W. Lee, R. J. Wallace, S. Weber, H. J. Lee, A. L. Kritcher, R. Falcone, S. P. Regan, H. Sawada, D. D. Meyerhofer, G. Gregori, C. Fortmann, V. Schwarz, R. Redmer, Compton scattering measurements from dense plasmas, *J. Phys. Conf. Ser.* 112 (2008) 032071.
- [9] H. J. Lee, P. Neumayer, J. Castor, T. Döppner, R. W. Falcone, C. Fortmann, B. A. Hammel, A. L. Kritcher, O. L. Landen, R. W. Lee, D. D. Meyerhofer, D. H. Munro, R. Redmer, S. P. Regan, S. Weber, S. H. Glenzer, X-ray Thomson scattering measurements of density and temperature in shock-compressed beryllium, *Phys. Rev. Lett.* (accepted).
- [10] J. Chihara, Interaction of photons with plasmas and liquid metals - photoabsorption and scattering, *J. Phys.: Condens. Matter* 12 (3) (2000) 231–247.
- [11] H. A. Baldis, J. Dunn, M. E. Foord, W. Rozmus, Thomson scattering diagnostic of solid density plasmas using x-ray lasers, *Rev. Sci. Instrum.* 73 (12) (2002) 4223–4228.
- [12] W. Ackermann, G. Asova, V. Ayvazyan, A. Azima, N. Baboi, J. Bähr, V. Balandin, B. Beutner, A. Brandt, A. Bolzmann, R. Brinkmann, O. I. Brovko, M. Castellano, P. Castro, L. Catani, E. Chiadroni, S. Choroba, A. Cianchi, J. T. Costello, D. Cubaynes, J. Dardis, W. Decking, H. Delsim-Hashemi, A. Delserieys, G. D. Pirro, M. Dohlus, S. Düsterer, A. Eckhardt, H. T. Edwards, B. Faatz, J. Feldhaus, K. Flöttmann, J. Frisch, L. Fröhlich, T. Garvey, U. Gensch, C. Gerth, M. Görler, N. Golubeva, H.-J. Grabosch, M. Grecki, O. Grimm, K. H. U. Hahn, J. H. Han, K. Honkavaara, T. Hott, M. Hüning, Y. Ivanisenko, E. Jaeschke, W. Jalmuzna, T. Jezynski, R. Kammering, V. Katalev, K. Kavanagh, E. T. Kennedy, S. Khodyachykh, K. Klöse, V. Kocharyan, M. Körfer, M. Kollwe, W. Koprek, S. Korepanov, D. Kostin, M. Krasilnikov, G. Kube, M. Kuhlmann, C. L. S. Lewis, L. Lilje, T. Limberg, D. Lipka, F. Löhler, H. Luna, M. Luong, M. Martins, M. Meyer, P. Michelato, V. Miltchev, W. D. Möller, L. Monaco, W. F. O. Müller, O. Napieralski, O. Napoly, P. Nicolosi, D. Nölle, T. Nuñez, A. Oppelt, C. Pagani, R. Paparella, N. Pchalek, J. Pedregosa-Gutierrez, B. Petersen, B. Petrosyan, G. Petrosyan, L. Petrosyan, J. Pflüger, E. Plönjes, L. Poletto, K. Pozniak, E. Prat, D. Proch, P. Pucyk, P. Radcliffe, H. Redlin, K. Rehlich, M. Richter, M. Roehrs, J. Roensch, R. Romaniuk, M. Ross, J. Rossbach, V. Rybnikov, M. Sachwitz, E. L. Saldin, W. Sandner, H. Schlarb, B. Schmidt, M. Schmitz, P. Schmüser, J. R. Schneider, E. A. Schneidmiller, S. Schnepf, S. Schreiber, M. Seidel, D. Sartore, A. V. Shabunov, C. Simon, S. Simrock, E. Sombrowski, A. A. Sorokin, P. Spanknebel, R. Spesyvtsev, L. Staykov, B. Steffen, F. Stephan, F. Stulle, H. Thom, K. Tiedtke, M. Tischer, S. Toleikis, R. Treusch, D. Trines, I. Tsakov, E. Vogel, T. Weiland, H. Weise, M. Wellhöfer, M. Wendt, I. Will, A. Winter, K. Wittenburg, W. Wurth, P. Yeates, M. V. Yurkov, I. Zagorodnov, K. Zapfe, Operation of a free-electron laser from the extreme ultraviolet to the water window, *Nature Photonics* 1 (2007) 336–342.
- [13] A. Höll, T. Bornath, L. Cao, T. Döppner, S. Düsterer, E. Förster, C. Fortmann, S. Glenzer, G. Gregori, T. Laarmann, K.-H. Meiwes-Broer, A. Przystawik, P. Radcliffe, R. Redmer, H. Reinholz, G. Röpke, R. Thiele, J. Tiggesbümker, S. Toleikis, N. Truong, T. Tschentscher, I. Uschmann, U. Zastra, Thomson scattering from near-solid density plasmas using soft x-ray free electron lasers, *J. High Energy Density Phys.* 3 (1-2) (2007) 120–130.
- [14] G. Gregori, A. Ravasio, Höll, S. H. Glenzer, S. J. Rose, Derivation of the static structure factor in

- strongly coupled non-equilibrium plasmas for x-ray scattering studies, *High Energy Density Phys.* 3 (2007) 99–108.
- [15] S. Sahoo, G. F. Gribakin, G. S. Naz, J. Kohanoff, D. Riley, Compton scatter profiles for warm dense matter, *Physical Review E (Statistical, Nonlinear, and Soft Matter Physics)* 77 (4) (2008) 046402.
- [16] R. Redmer, H. Reinholz, G. Röpke, R. Thiele, A. Höll, Theory for x-ray thomson scattering in dense plasmas, *IEEE Trans. Plasma Sc.* 33 (2005) 77–84.
- [17] R. Thiele, R. Redmer, H. Reinholz, G. Röpke, Using the gould-dewitt scheme to approximate the dynamic collision frequency in a dense electron gas, *J. Phys. A* 39 (17) (2006) 4365–4368.
- [18] C. Fortmann, T. Bornath, R. Redmer, H. Reinholz, G. Röpke, V. Schwarz, R. Thiele, X-ray thomson scattering cross-section in strongly correlated plasmas, *Laser Part. Beams* (submitted).
- [19] B. Holst, R. Redmer, M. P. Desjarlais, Thermophysical properties of warm dense hydrogen using quantum molecular dynamics simulations, *Phys. Rev. B* 77 (18) (2008) 184201.
- [20] B. L. Henke, E. M. Gullikson, J. C. Davis, X-ray interactions: photoabsorption, scattering, transmission, and reflection at $e=50$ -30000 eV, $z=1$ -92, *At. Data Nucl. Data Tables* 54 (1993) 181 – 342.
- [21] J. J. MacFarlane, I. E. Golovkin, P. R. Woodruff, Helios-cr a 1-d radiation-magnetohydrodynamics code with inline atomic kinetics modeling, *J. Quant. Spectrosc. Radiat. Transfer* 99 (2006) 381.
- [22] L. Cao, I. Uschmann, F. Zamponi, T. Kämpfer, A. Fuhrmann, E. Förster, A. Höll, R. Redmer, S. Toleikis, T. Tschentscher, S. Glenzer, Space-time characterization of laser plasma interactions in the warm dense matter regime, *Laser and Particle Beams* 25 (02) (2007) 239 – 244.